

# THE TWO-HEMISPHERE CONVECTION MODEL BASED ON STATISTICAL MAPS OF FIELD-ALIGNED CURRENT DERIVED FROM HIGH-PRECISION SATELLITE MAGNETIC FIELD DATA

R. Lukianova <sup>(1)</sup>, F. Christiansen <sup>(2)</sup>

<sup>(1)</sup>*Arctic & Antarctic Research Institute  
38 Bering Street, St.Petersburg 199397, Russia  
Email: renata@aari.nw.ru*

<sup>(2)</sup>*DTU Space  
Juliane Maries Vej, 30 DK 2100 Copenhagen, Denmark  
Email: fch@space.dtu.dk*

## ABSTRACT

A new approach for modeling the global distribution of ionospheric electric potentials utilizing high-precision maps of FACs derived from measurements by the Ørsted, Champ, Magsat satellites as input to a comprehensive numerical scheme is presented. The boundary conditions provide a correct treatment of the asymmetry of conductivity and sources of electric potential between the northern and southern hemispheres. On the basis of numerical simulation the basic convection patterns developed simultaneously in both hemispheres for equinox and summer/winter solstices are obtained. A rather complicated dependence of the convection patterns on season linked with the sign of IMF BY is found.

## 1. INTRODUCTION

A comprehensive study of field-aligned current (FAC) distribution was carried out due to the emergence of a new generation of low-orbiting satellites with high-precision magnetometers (Orsted, Champ, Magsat). These spacecrafts are providing an enormous database of magnetic field variations above the ionosphere, resulting in the appearance of qualitatively new FAC model [10]. This motivates us to attempt a new approach for modeling the global distribution of the ionospheric electric potential utilizing the detailed maps of FAC as an input for a comprehensive numerical scheme [5]. Since the FAC model [10] is fully parameterized by the IMF direction/strength, by season, and by hemisphere, the same parameterization is further applied for the convection model. In our approach the boundary conditions provide a correct treatment of the asymmetry in conductivity and sources of electric potential (i.e. FAC) between the northern and southern hemispheres accounting for the mutual electrodynamic influence of the opposite hemispheres. As the inter-hemispheric asymmetry in the FAC and conductivity distributions is a common feature of ionospheric electrodynamics, the effect of electrical coupling between hemispheres can be significant. As a result, it appears the convection patterns developed simultaneously in the opposite hemispheres to be different but not independent from each other. The model also handles the electric field far below the auroral latitudes. It allows a simulation of the electric field disturbances that originate at the polar regions but cover a broad range of latitudes in both hemispheres.

In this paper we give brief description of the statistical model of FAC (Section 2). The convection model including the statement of the problem and boundary conditions is described in Section 3. In Section 4 the model capability is demonstrated. In particular, we focus on the effect of significant inter-hemispheric asymmetry in the polar regions governed by the IMF clock angle and solar zenith angle. The electric fields located below the polar cap boundary are presented. The final Section 5 is a summary.

## 2. FIELD-ALIGNED CURRENT MODEL

Since the early results [4], no comprehensive studies of FAC distribution were carried out, until the emergence of a new generation of low-orbiting satellites with high-precision magnetometers (Orsted, Champ). These spacecrafts are providing an enormous database of magnetic field variations above the ionosphere, resulting in the appearance of qualitatively new FAC model parameterized by the IMF direction/ strength, by season, and by hemisphere [10]. The FACs are determined directly by a simple 2-D curl technique combined with fitting of spherical harmonic functions. The model is limited to  $|B|=12$  nT as data coverage is too poor above this value and it is not valid for periods of rapid changes of the magnetosphere configuration as during magnetic storms and substorms. Fig. 1 adopted from [10] gives examples of FAC distribution for

$BT = \sqrt{BZ^2 + BY^2} = 5 \text{ nT}$  over the northern winter and southern summer polar regions (Fig. 1a). For each season and both hemispheres experimental FAC distributions are obtained for eight IMF clock-angles. The plots are organized according to the IMF clock-angle in GSM Y- Z plane shown in Fig. 1a on the right. Fig. 2b shows the same but for equinox. For modeling the global distribution of the ionospheric electric potential these high-precision maps of FACs are utilized. Since the FAC model is fully parameterized by the IMF conditions, by season, and by hemisphere, the same parameterization is further applied for the convection model.

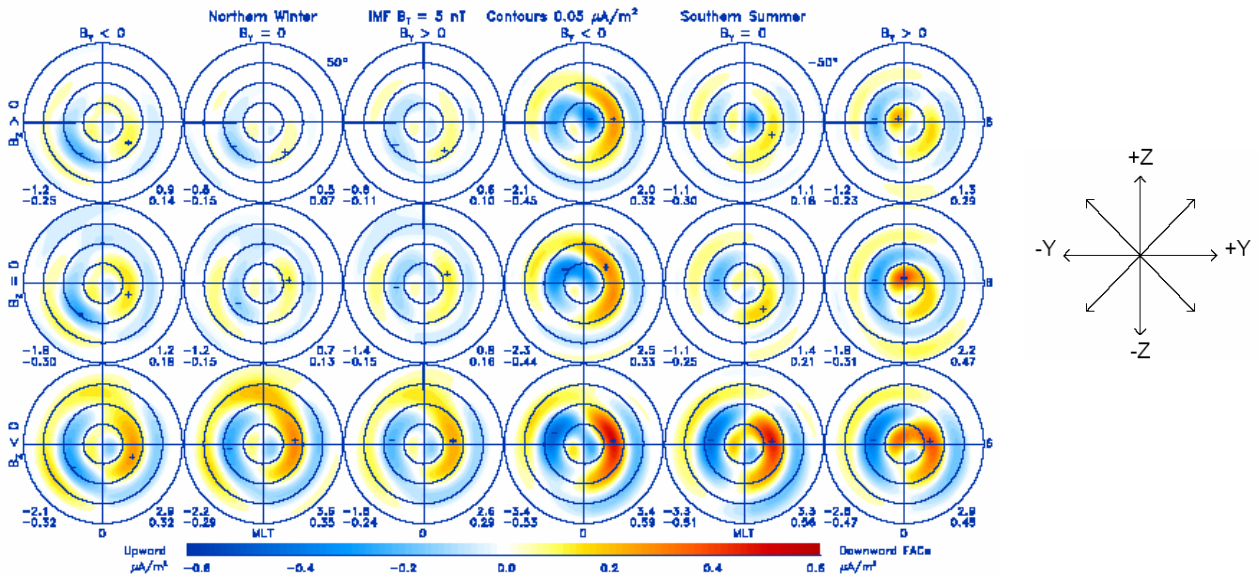


Fig. 2a. Maps of FAC for  $BT = 5 \text{ nT}$  organized by the IMF clock angle for northern winter (left) and southern summer (right). The central plots are the patterns for  $BT = 0$ . The total hemispherical currents (top numbers, MA) and the minimum and maximum current densities (lower numbers, mA/m<sup>2</sup>) are marked at the bottom corners of each polar subplot. The upward currents are negative and downward - positive. The FACs min/max density locations are identified by “-“ and “+”.

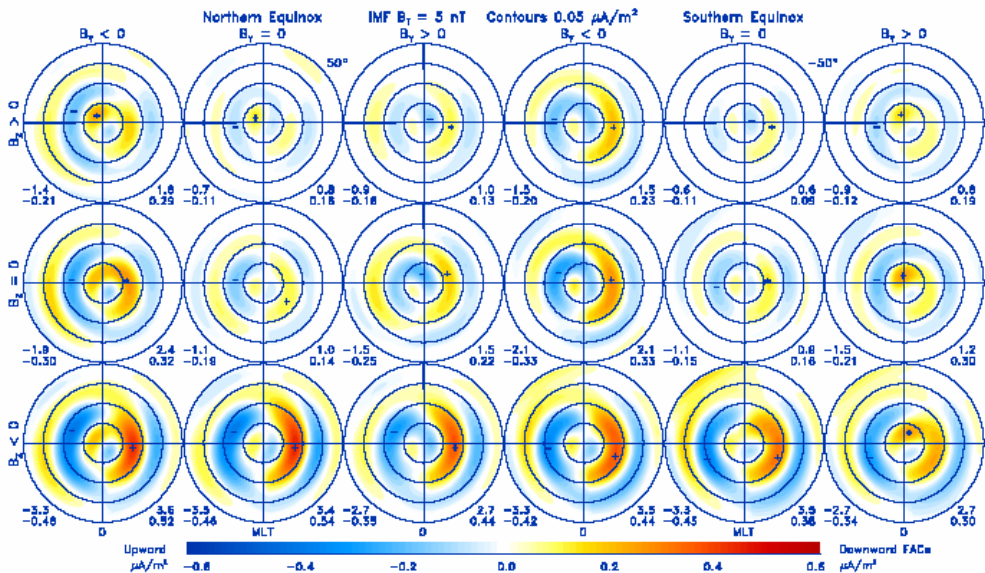


Fig. 2b. The same but for equinox.

### 3. FAC-BASED CONVECTION MODEL

**Statement of the problem.** The equation of electric current continuity:

$$\text{div } \mathbf{J} = j'' \cdot \sin \chi \quad (1)$$

where  $\mathbf{J}$  is the height-integrated horizontal ionospheric current,  $j''$  is the FAC intensity,  $\chi$  is the magnetic inclination, is solved on a grid covering the two-dimensional ionospheric shell with specified height-integrated conductivity. The electrical conjugacy between northern and southern polar caps via the geomagnetic field is negligible. Outside of the polar caps the electrodynamic coupling between opposite hemispheres is taken into account, the closed geomagnetic field lines being supposed equipotential for conjugate points. The appropriate boundary conditions connect the regions of open and closed field lines, providing a self-consistent solution of (1). Fig. 3 gives a sketch of the ionospheric shell. Fig.3a shows how the whole shell is divided into three subregions: northern ( $\alpha=1$ ) and southern ( $\alpha=2$ ) polar caps with boundaries at the colatitudes  $\theta_1$  and  $\theta_2=\pi-\theta_1$ , respectively. The polar are uncoupled with respect to electric potential. On the remaining portion of the sphere the closed geomagnetic field lines are taken to be equipotential for conjugate points on opposite hemispheres. This allows us to solve Eq. (1) on each half of the lower-latitude region. For definiteness, let it be the northern half ( $\alpha=3$ ) from the polar boundary at  $\theta_1$  to a specified equator boundary at  $\theta_3$  (this area is denoted by “N” in the sketch). The boundary  $\theta_3$  is set latitudinally away from the equator to avoid a division by zero in the expression for the components of conductivity tensor. The sum of conductivities and sources (FAC) at conjugate points of “N” and “S” is used at each point of ( $\alpha=3$ ) region. Thus for the ionospheric shell, we obtain the following boundary value problem:

$$\text{div } \mathbf{J}_1 = j_1 \quad \text{for } \theta \leq \theta_1 \quad (2)$$

$$\text{div } \mathbf{J}_2 = j_2 \quad \text{for } \pi - \theta_1 \leq \theta < \pi \quad (3)$$

$$\text{div } \mathbf{J}_3 = j_3 \quad \text{for } \theta_1 \leq \theta \leq \theta_3 \quad (4)$$

where  $J_\alpha$  is the height-integrated horizontal ionospheric current,  $j_\alpha$  is the radial component of FACs in the corresponding subregion indicated by  $\alpha = 1, 2, \text{ and } 3$ .

**Boundary conditions.** As illustrated in Fig. 3b, the whole system schematically looks like the two upside-down caps, one into another put on the one upside-down saucer, in such a way that all three boundaries are at a common latitudinal circle. The boundary conditions of the three subregions ( $\alpha = 1, 2, 3$ ) are

$$U_1(\theta_1, \varphi) = U_3(\theta_1, \varphi) = U_2(\theta_2, \varphi) \quad (5)$$

$$J_1(\theta_1, \varphi) - J_3(\theta_1, \varphi) = J_2(\theta_2, \varphi) \quad (6)$$

$$J_3(\theta_3, \varphi) = 0 \quad (7)$$

where  $U_\alpha$  is the ionospheric electric potential in the corresponding subregion. Boundary condition (5) means that there is no discontinuity in the electric potential across the boundary of the polar cap and between the boundaries of opposite caps. In calculation scheme, both the northern cap ( $\theta_1$ ) and southern cap ( $\theta_2$ ) boundaries border on the common region ( $\alpha = 3$ ). Condition (6) means that any possible discontinuities of the longitudinal components of ionospheric currents across the boundaries of the northern and southern caps compensate each other through the currents leaking across these boundaries into the lower latitudes. Condition (7) means the absence of current across the equator.

**Numerical algorithm.** The quantities  $U_\alpha$  and  $J_\alpha$  are connected by the Ohm's law:

$$\mathbf{J}_\alpha = \sum_\alpha \cdot (-\nabla U_\alpha) \quad (8)$$

where  $\sum_\alpha$  is the height-integrated conductivity tensor including both Hall and Pedersen conductivity. Eqs. (2) – (7) are transformed to a discrete form on the grid and solved numerically using an iteration technique, giving the potential as a function of conductance and FAC distribution. The coordinate grid steps were taken as  $\Delta\theta=1^\circ$  and  $\Delta\varphi = (360/128)^\circ$ . Two parameters serve as the models' input: maps of FAC and maps of conductivity, with both the solar and auroral precipitation contribution [11, 3] included. The conductivity is controlled by four parameters: the Kp index, the 10.7 cm solar radio flux proxy (F107), day of the year (DOY) and UT.

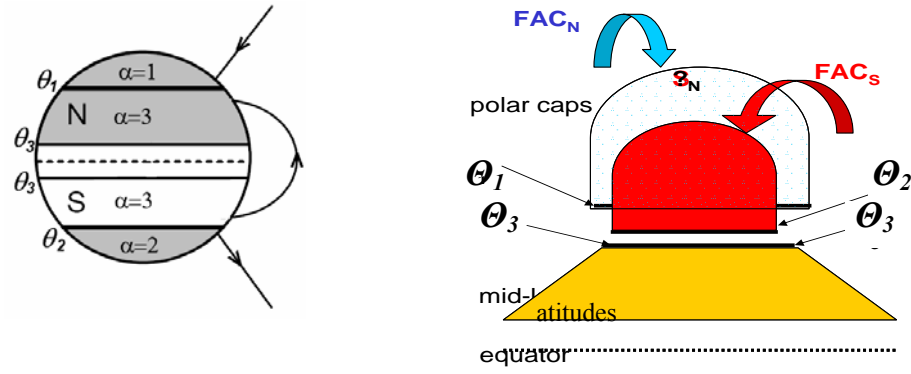


Fig. 3. Left: Sketch of the division of the ionospheric shell into three regions: northern, southern polar caps and the mid-latitude region. Arrows represent the geomagnetic field lines. Calculation area is shaded. Right: Scheme illustrating the electrodynamic coupling between the opposite polar caps and the mid-latitude region.

### 3. MODELING RESULTS

**FAC, conductivity and electric potential distributions.** Depending on the conductivity and FAC distribution, the solution of Eq (1) gives the corresponding electric potential distribution. Fig. 4 shows an example of FAC, Pedersen conductivity and electric potential distribution in both polar regions, when the IMF  $BZ > 0$ ,  $BY < 0$ ,  $BT = 5$  nT. Other input parameters are taken  $DOY = 350$  (northern winter solstice),  $UT = 10:30$ ,  $F10.7 = 120$ ,  $Kp = 1$ . The upper and lower rows of plots show the northern winter and southern summer, respectively. The statistical maps of FAC [10] are the first ones which describes quantitatively the intense polar cap FAC related to the sign of IMF  $BY$ . Consequently, the FAC-based convection model is able to describe large and variable electric fields in the polar cap, which appear due to the IMF  $BY$ -related effect. The intra- and inter-hemispheric asymmetry in distribution of the ionospheric electrodynamic parameters is primarily originated from the interplay of the two factors, namely the IMF  $BY$  and the solar zenith angle (its seasonal and diurnal variations). In particular, it is seen in Fig. 4 that the shape of the corresponding cells from the opposite hemispheres are recognizably different for the same IMF orientation. In particular, the winter dusk cell generally dominates and in the dayside near-pole region an isolated convection cell extended from the prenoon is identified. During southern summer the convection vortex mostly surrounds the pole. In general, the modeling results confirm that a change of the IMF  $BY$  sign does not produce a simple mirror antisymmetric change in convection patterns within the same hemisphere [5, 7, 8] as well as a symmetric response in the opposite hemispheres [5, 6].

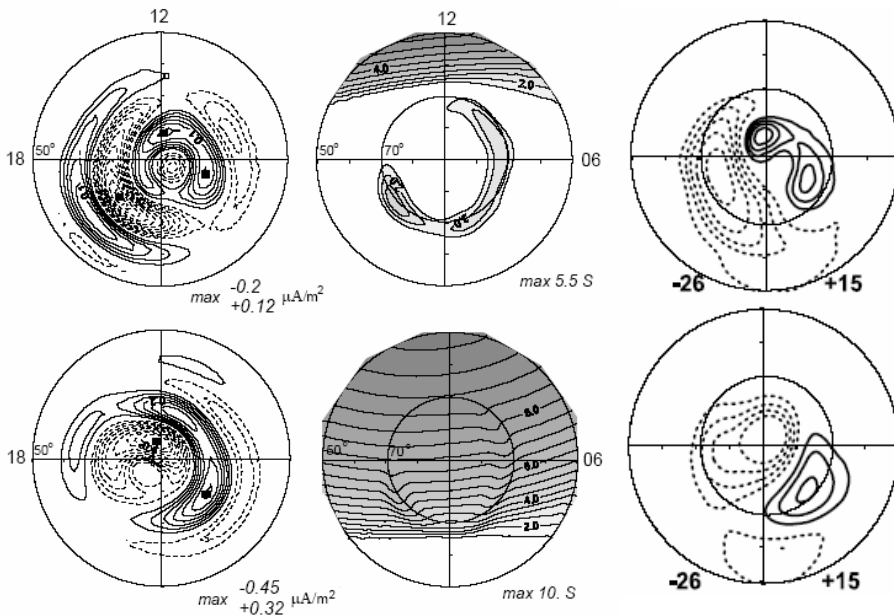


Fig. 4. Maps of FAC, Pedersen conductivity and electric potential distribution for the IMF  $BZ > 0$ ,  $BY < 0$ ,  $BT = 5$  nT,  $DOY = 350$ ,  $UT = 1030$ ,  $F10.7 = 120$ ,  $Kp = 1$  for the northern winter (top) and southern summer polar regions (bottom). Densities of the downward and

upward FAC are shown by solid and dotted isolines, respectively. The maxima current densities, conductance and electric potential are marked at the bottom corners of corresponding plot.

**Lower latitudes.** One of the unresolved problems of ionospheric modeling is the determination of the electric fields penetrating to middle latitudes, since this field is located below the outer boundary of the existed models. In the frame of FAC-based convection model the electric field as low in latitude as  $30^\circ$  from the equator can be reproduced. The westward and equatorward electric field component are calculated as follows:

$$E_\theta = -\partial U / \partial \theta \quad (9)$$

$$E_\varphi = 1 / \sin \theta \cdot \partial U / \partial \varphi \quad (10)$$

As an example, in Fig. 5 we present the variations of zonal and meridional component of the electric field that determines the plasma motion along the latitude and longitude, respectively, under southward IMF conditions,  $B_y=0$  for equinox and northern winter. Figure 6 indicates that both components effectively penetrate to the region of closed geomagnetic field lines where its behavior is controlled by the electric potential distribution in both polar caps. The night-time electric field penetrates further comparing to the day-time one. This effect is clearly seen during as equinox as solstice. The notable feature is that a stronger winter electric field decays more rapidly with latitude than a weaker summer field. The MLT-profile of the westward and equatorward components obtained from the present model is close to the variations derived from a Rise Convection Model (e.g., [1]), providing an independent check of our model.

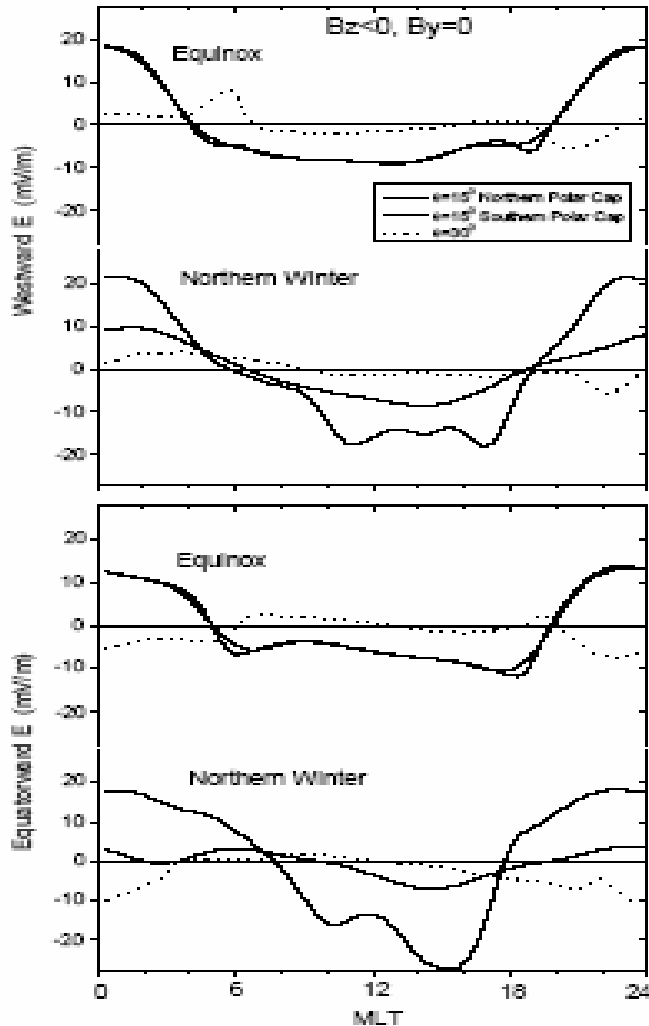


Fig. 5. Westward (top) and equatorward (bottom) components of the electric field in the northern and southern polar caps ( $\theta = 15^\circ$ ), and at subauroral latitudes ( $\theta = 32^\circ$ ) for the equinox and northern winter.

#### 4. FINAL REMARKS

We have performed numerical modeling of the global distribution of ionospheric electric field. A new approach is to utilize realistic maps of FACs obtained from Ørsted, Champ and Magsat satellites [10] as an input for the calculation of convection systems which are developed simultaneously in both hemispheres. On the basis of numerical simulation the basic convection patterns for different seasons under various IMF conditions were obtained. These showed all common features inherent in recent statistical models based on different instrumentation, e.g., on ground magnetometers data scaled by DMSP satellite observations [9], on DE2 satellite observations [13], on the radar measurements [12]. Also, quantitative comparison of the modeling convection flow and the EISCAT observations in the polar cap also showed a good agreement [8]. In the frame of FAC-based convection model some new remarkable features were reproduced. In particular, the results demonstrated how the mutual influence of opposite hemispheres can modify the global convection and confirmed the necessity to link season with the sign of IMF BY to fully characterize the dependence.

The main goal of our work is to produce a flexible model of the ionospheric electrodynamics that is able to reproduce the FAC and convection patterns with great accuracy for a variety of scientific and practical applications. Currently, the technique of space measurements of FACs is developing rapidly. Recently, the magnetic field data obtained from the low-precision magnetic data from Iridium constellation were used to extend studies that infer the dependence of the global FAC configuration on IMF direction and magnitude, hemisphere and season [2]. It is believed that further development of high-precision measurements of FACs, in particular by the SWARM satellites will help to collect more information and to cover a wider range of IMF/SW conditions, which in turn, will provide an opportunity to improve the FAC and electric field modeling.

**ACKNOWLEDGMENTS.** The authors greatly appreciate the contribution of V. Papitashvili.

#### REFERENCES

- [1] B. G. Fejer, and J. T. Emmert, "Low-latitude ionospheric disturbance electric field effects during the recovery phase of the 19–21 October 1998 magnetic storm," *J. Geophys. Res.*, 108(A12), pp. 1454, doi:10.1029/2003JA010190, 2003.
- [2] D. L. Green, C. L. Waters, B. J. Anderson, and H. Korth, "Seasonal and interplanetary magnetic field dependence of the field-aligned currents for both Northern and Southern Hemispheres," *Ann. Geophys.*, 27, pp. 1701–1715, 2009.
- [3] D. A. Hardy, M. S. Gussenhoven, R. Raistrick, and W. J. McNeil, "Statistical and functional representation of the pattern of auroral energy flux, number flux and conductivity," *J. Geophys. Res.*, 92, pp. 12,275, 1987.
- [4] T. Iijima, and T. A. Potemra, "Large-scale characteristics of field-aligned currents associated with substorm," *J. Geophys. Res.*, 81, pp. 3999, 1976.
- [5] R. Lukianova, and F. Christiansen, "Modeling of the global distribution of ionospheric electric fields based on realistic maps of field-aligned currents," *J. Geophys. Res.*, 111, A03213, doi:10.1029/2005JA011465, 2006.
- [6] R. Lukianova, and F. Christiansen, "Modeling the UT-effect in global distribution of ionospheric electric fields," *J. Atmos. Solar-Terr. Phys.* 70 (2-4), pp. 637–645, 2008.
- [7] R. Lukianova, C. Hanuise, and F. Christiansen, "Asymmetric distribution of the ionospheric electric potential in the opposite hemispheres as inferred from the SuperDARN observations and FAC-based convection model," *J. Atmos. Solar-Terr. Phys.*, 70, pp. 2324-2335, doi:10.1016/j.jastp.2008.05.015, 2008a.
- [8] R. Lukianova, A. Kozlovsky, and T. Turunen, "Comparison and validation studies related to the modeling ionospheric convection and the EISCAT observations in the polar cap," *Int. J. Geomagnetism Aeronomy*, Vol. 7, No 3, G13005, doi:10.1029/2007GI000169, 2008b.
- [9] V. O. Papitashvili, and F. J. Rich, "High-latitude ionospheric convection models derived from Defense Meteorological satellite Program ion drift observations and parameterized by the interplanetary magnetic field strength and direction," *J. Geophys. Res.*, 107(A8), pp. 1198, doi:10.1029/2001JA000264, 2002.
- [10] V. O. Papitashvili, F. Christiansen, and T. Neubert, "A new model of field-aligned currents derived from high-precision satellite magnetic field data," *Geophys. Res. Lett.*, 29(14), pp. 1683, doi:10.1029/2001GL014207, 2002.
- [11] R. M. Robinson, and R. R. Vondrak, "Measurements of E region ionization and conductivity produced by solar illumination at high latitudes," *J. Geophys. Res.*, 89, pp. 3951, 1984.
- [12] J. M. Ruohoniemi, and R. A. Greenwald, "Dependencies of high-latitude plasma convection: Consideration of IMF, seasonal, and UT factors in statistical patterns," *J. Geophys. Res.*, 110, A09204, doi:10.1029/2004JA010815, 2005.
- [13] D. R. Weimer, "Improved ionospheric electrodynamic models and application to calculating Joule heating rates," *J. Geophys. Res.*, 110, A05306, doi:10.1029/2004JA010884, 2005.